

pubs.acs.org/acscatalysis Research Article

Kinetic Study of the Hydrogenation of Unsaturated Aldehydes Promoted by CuPt_x/SBA-15 Single-Atom Alloy (SAA) Catalysts

Yueqiang Cao, Jonathan Guerrero-Sańchez, Ilkeun Lee, Xinggui Zhou, Noboru Takeuchi, and Francisco Zaera*



Cite This: ACS Catal. 2020, 10, 3431-3443



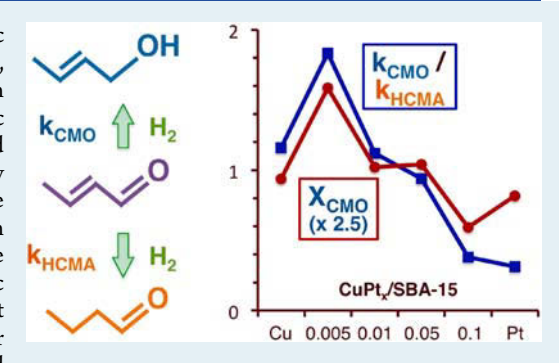
ACCESS

III Metrics & More

Article Recommendations

Supporting Information

ABSTRACT: A comprehensive study of the kinetics of the catalytic hydrogenation of unsaturated aldehydes, in particular of cinnamaldehyde, promoted by $\text{CuPt}_x/\text{SBA-15}$ single-atom alloy catalysts was carried out in order to identify trends as a function of the composition of the bimetallic nanoparticles, that is, of the value of x. The optimum performance reported by us recently [ACS Catal. 2019, 9, 9150–9157] in terms of selectivity toward the formation of cinnamyl alcohol, the desired product, by the catalyst with x=0.005 was corroborated. A rapid decrease was seen in catalytic activity in batch reactors with all catalysts, in particular with pure Cu/SBA-15. This was ascribed, based on DFT calculations and microkinetic simulations, to the relative weak adsorption of the reactant compared to that of the products, which leads to the blocking of catalytic sites by the latter early on in the catalytic runs. It was determined that selectivity is controlled



by the relative values of the initial rate constants for hydrogenation to the unsaturated alcohol versus the saturated aldehyde. Those were found to vary by up to an order of magnitude as a function of Pt content in the catalyst, in spite of the fact that the hydrogenation steps are presumed to occur on Cu, not Pt, sites. In general, significant changes in equilibrium and kinetic parameters were seen across the series of catalysts tested (versus x), indicating that the addition of even small amounts of Pt to these Cu single-atom alloy (SAA) catalysts affects the intrinsic performance of the hydrogenation catalytic sites.

KEYWORDS: selective hydrogenation, unsaturated aldehydes, alloy catalysts, platinum, copper, kinetics

1. INTRODUCTION

Single-atom heterogeneous catalysis (SACs) has gained quite a bit of notoriety in recent years as a way to introduce well-defined sites to control activity and/or selectivity in the catalytic promotion of reactions. One particular class of such SACs is so-called single-atom alloy (SAA) catalysts, which consist of bimetallic nanoparticles (NPs) dispersed on a solid support comprised of one dominant metal mixed with a small amount of a second, highly diluted and presumably dispersed as single atoms. These catalysts have been tested for the promotion of a number of reactions 12-16 and have proven particularly useful for the selective hydrogenation of organic reactants.

In SAA catalysts, the majority metal is usually selected based on its unique properties for the promotion of specific chemical steps. In the case of hydrogenation reactions, coinage metals (Cu, Ag, Au) are often picked, in many cases as a way to prevent dehydrogenation and other decomposition steps but also because they may favor particular adsorption geometries for the reactants that can lead to kinetic control of selectivity. For instance, we have recently shown that Cu surfaces tend to adsorb unsaturated aldehydes via their terminal carbonyl group, thus facilitating the hydrogenation of the C=O bond in

the presence of other unsaturations such as C=C bonds. ¹⁶ This leads to the selective production of unsaturated alcohols, which are highly desirable products. ^{17–19}

The main limitation with coinage metals is that they are quite ineffective at advancing the first step in hydrogenation processes, the activation of molecular hydrogen to produce adsorbed hydrogen atoms. For that, a small amount of another (minority) metal, often noble transition metals such as Pd or Pt, can be added. The premise is that these can easily help with the dissociative adsorption of H₂. Small amounts are required, however, because otherwise they can dominate the whole hydrogenation process and therefore reduce its selectivity. The presumption in SAA catalysts is that this minority element is present on the surface in a dilute and atomic form.

The fact that such dilute bimetallic systems can exhibit the desired chemistry has been nicely tested by the Sykes group at

Received: December 13, 2019
Revised: February 11, 2020
Published: February 27, 2020



Tuffs University using model single-crystal and a combination of surface-sensitive techniques under ultrahigh vacuum (UHV) conditions. In their initial report, they demonstrated that individual Pd atoms on a Cu(111) single-crystal surface are indeed capable of dissociating $\rm H_2$ provided from the gas phase and to produce individual adsorbed H atoms that then spill over to the Cu substrate. 20 They also showed that such H(ads) can be used to hydrogenate unsaturated organic reactants adsorbed on the Cu(111) surface. In subsequent work, additional experimental evidence was acquired for this model, $^{8,9,11,13,21-23}$ and supporting quantum mechanics calculations were added. 9,11,21,22,24,25

In collaboration with the Maria Flytzani-Stephanopolous group, Sykes and co-workers have also proven that SAA catalysts can selectively promote a number of catalytic reactions.^{8,9,13} By combining the two sets of experiments, they used their surface-science research to provide a working model to explain the SAA catalytic behavior. Unfortunately, the information obtained from studies under UHV cannot always be directly translated into surfaces exposed to atmospheric pressures of reactants. It is well-known that the composition of solid surfaces can be modified by annealing to high temperatures or by exposing them to reactive gases; segregation of specific atoms from the bulk into the surface or vice versa is a common occurrence.²⁶ In the specific case of Cu-Pt SSA catalysts, we have recently reported that their Cu surface may become partially oxidized under reaction conditions and that the resulting thin CuO, film may push the Pt atoms into the subsurface. 16 Evidence for a similar interpretation, including CO-IR absorption spectroscopy data obtained in situ during the hydrogenation of acrolein that can be associated with the CuO, layer, has been provided by other groups as well, 10 and analogous behavior has also been identified by X-ray absorption with supported Cu-Pt and Au-Pd NPs exposed to CO or H₂ atmospheres.²⁷ With model systems, direct spectroscopic (temperature-programmed desorption, IR absorption spectroscopy, X-ray photoelectron spectroscopy) measurements have highlighted the mobility of Pt atoms in and out of the surface of Cu(111) crystals (and of Cu atoms in and out of Pt(111) crystals) under CO atmospheres.^{28,29} Finally, virtually no catalytic promotion of H-D scrambling with $H_2 + D_2$ mixtures could be detected with $CuPd_x$ films until reaching x values above approximately 0.2, a result that points to a potential limitation in terms of availability of atoms of the second metal in SAA catalysts on the surface.3

The discussion above points to the caution that needs to be exerted when extrapolating results obtained with model systems to more realistic catalysts and processes. Ideally, the catalysts need to be characterized in situ (or in operando mode) under conditions resembling those present during catalysis to obtain direct structure-reactivity correlations. Our group is in the process of performing such experiments. Alternatively, some information can be obtained indirectly via the careful characterization of the kinetics of catalytic reactions. That is what we have done here for the case of the hydrogenation of cinnamaldehyde (CMA) promoted with CuPt_r/SBA-15 catalysts. As reported previously by us, this reaction exhibits optimum performance in terms of selectivity toward the production of the unsaturated alcohol (cinnamyl alcohol, CMO) with Cu catalysts containing small amounts of Pt, specifically with a CuPt_{0.005}/SBA-15 catalyst. 16 We here trace that optimum performance to a higher value of the reaction rate constant for the hydrogenation of CMA to CMO relative to that of its conversion to the saturated aldehyde (3-phenylpropanal, HCMA). Interestingly, those two constants, as well as the equilibrium constants associated with the adsorption of the reactants and products, vary by about an order of magnitude as the Pt content is varied, even if many of the associated steps are supposed to take place on Cu sites. This effect must reflect a collective (nonlocalized) modification of the electronic structure of the surface even at the low-Pt-content limit. There is clearly a synergy between the Cu and Pt atoms that contributes to the modification of the catalytic properties of these so-called SAA catalysts.

2. EXPERIMENTAL DETAILS

All catalysts were prepared by incipient-wetness impregnation of commercial SBA-15 (ACS Material) using copper nitrate (Cu(NO₃)₂·3H₂O, Sigma-Aldrich, 98% purity) and chloroplatinic acid ($H_2PtCl_4 \cdot 6H_2O$, Sigma-Aldrich, $\geq 37.50\%$ Pt basis), as described in a previous publication. 16 The nominal loading of Cu was 5 wt % in all cases, and the Pt/Cu molar ratio, x, was set by tuning the amount of added chloroplatinic acid; here we will refer to these catalysts as CuPt_r/SBA-15. The impregnated samples were kept at room temperature for 24 h, dried at about 350 K for 24 h, and grounded to make them into powder form. All catalysts were reduced at 625 K under H₂ for 3 h prior to their use. A total of 10 catalysts were prepared, for x = 0, 0.001, 0.005, 0.01, 0.05, 0.1, 0.2, 0.5, 0.75, and ∞ (pure Pt), even if kinetic data are reported here for seven of those only; the catalysts with the higher Pt content have been used elsewhere for additional physical characterization. 10

The metal loadings were quantified by inductively coupled plasma atomic emission spectrometry (ICP-AES), using a PerkinElmer Optima 7300DV ICP-OES apparatus that combines an SCD detector and an echelle optical system which enables the unit to measure all wavelengths simultaneously—in the ultraviolet wavelength range from 165 to 403 nm and in the visible wavelength range from 404 to 782 nm. The metal NPs size distributions were estimated from electron microscopy images taken using a scanning transmission electron microscopy (STEM) FEI Titan Themis 300 instrument equipped with a X-ray spectrometer for energy dispersion spectroscopy (EDS) imaging. 16 The NP crystallinity was evaluated by X-ray diffraction (XRD), using a Bruker D8 Advance Diffractometer with Cu K α radiation ($\lambda = 1.5406$ Å). Hydrogen temperature-programmed reduction (H₂-TPR) experiments were carried out on a Micromeritics Autochem II 2920 instrument.

The kinetic measurements were performed in a 300 mL high-pressure 4560 bench Parr batch reactor. Approximately 0.1 g of the catalyst was added to 75 mL of isopropanol (Sigma-Aldrich, ≥99.7% purity, used as the solvent), 0.8 g of CMA (Sigma-Aldrich, ≥95% purity), and 2 mL of benzyl alcohol (Sigma-Aldrich, 99.8% purity, an internal standard).3 The vessel was purged 5 times with 10 bar of H₂ (Liquid Carbonic, >99.995% purity) and then pressurized to the reaction H₂ pressure. The reaction mixture was heated to 375 K, the stirring was switched on, and the time was set to zero. The composition of the mixture was followed by extracting 1 mL aliquots at preset times and analyzing them using an Agilent 6890N gas chromatograph with an HP-50 column (15 m \times 320 μ m \times 0.25 μ m). The H₂ pressures during reaction were estimated from the initial measurements, taken at room temperature as the reactor was pressurized, corrected to

Table 1. Estimated and Actual Cu and Pt Metal Loadings of the CuPt_x/SBA-15 Catalysts Used in These Studies^a

Samples	Nominal Cu wt %	Measured Cu wt %	Estimated Pt wt %	Measured Pt wt %	Measured $x = Pt/Cu$		
Cu/SBA-15	5.00	4.60					
$CuPt_{0.001}/SBA-15$	5.00	4.64	0.014	0.015	0.0011		
$CuPt_{0.005}/SBA-15$	5.00	4.80	0.074	0.073	0.0049		
$\text{CuPt}_{0.01}/\text{SBA-15}$	5.00	4.73	0.146	0.148	0.010		
CuPt _{0.05} /SBA-15	5.00	4.65	0.716	1.04	0.068		
$CuPt_{0.1}/SBA-15$	5.00	4.63	1.426	2.01	0.12		
Pt/SBA-15			5.00	4.53			
^a The experimental values were determined by ICP-AES.							

CuPt_x/SBA-15 TEM & Particle Size Distributions

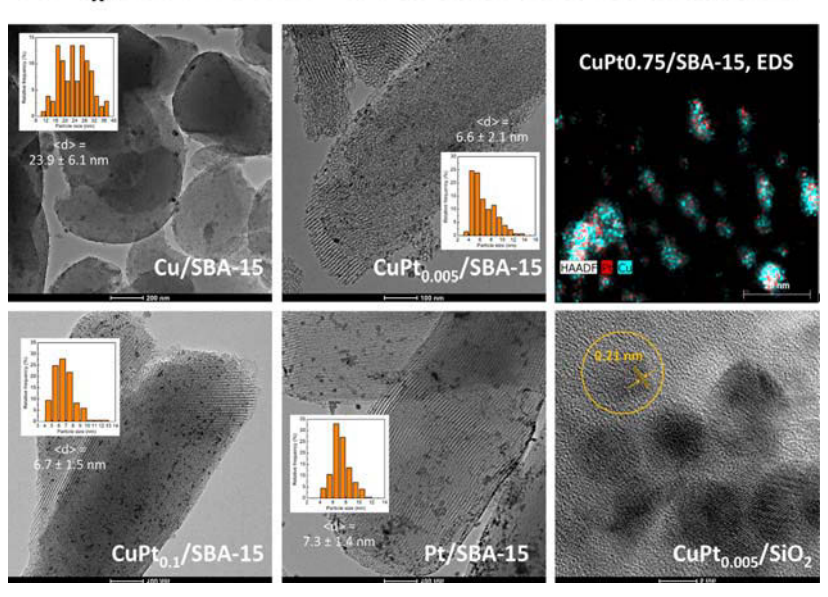


Figure 1. Left and center columns: STEM images of the indicated catalysts. Top, right: EDS image from a CuPt_{0.75}/SBA-15 sample, with the Pt and Cu atoms colored in red and blue, respectively (reproduced with permission from ref 16. Copyright 2019 American Chemical Society). Bottom, right: high-resolution TEM of the metal NPs for the CuPt_{0.005}/SBA-15 sample. Scale bars (from left to right): Top row: 200, 100, and 20 nm; Bottom: 100, 100, and 5 nm.

account for the heating to the reaction temperature using the ideal gas equation. For the recycling experiments reported in Figure 8, the reaction mixture, together with the suspended catalyst powder, was collected after each run and filtered to separate the catalyst from the spent solution; the collected solid was then returned to the reactor, and a new fresh reaction mixture added to initiate the next catalytic run. No other pretreatment steps were taken in between these consecutive runs.

Turnover numbers (TONs) and turnover frequencies (TOFs) were estimated in terms of molecules converted per surface metal atom (Cu or Pt) by using the NPs size distributions from TEM characterization of the catalysts, assuming spherical shapes and bulk metal densities. In these calculations the total number of metal atoms on the surface was used regardless of their nature, as no reliable way to estimate the individual surface coverages of Cu and Pt atoms was available; such an approach may make the meaning of the TOFs suspect, since the nature of the catalytic sites is also unknown. In this context, the fact that the Pt NPs display a wide distribution of sizes ($\Delta d \sim \pm 2$ nm in most cases, as indicated below) also introduces a source of error in our calculations. That effect is difficult to quantify as well, because

the consequences of changes in NP size to catalytic activity may manifest mainly as changes in the relative numbers of sites with different coordinations numbers, i.e., in terraces versus steps, kinks, and other defects. Although we argue that it may be better to view the kinetic data in terms of conversion versus time, ¹⁶ activity is here reported in TOFs nevertheless to follow standard conventions in catalytic studies. Ultimately, we emphasize that regardless of the units chosen to report catalytic activity, most of the conclusions reached below rely on relative comparisons across the family of catalysts used, and those are not affected by this choice.

The quantum mechanics calculations were carried out using periodic density-functional theory (DFT), as described in previous publications. 16,32,33 A Vienna ab initio simulation package was used, 34 with projector-augmented waves. 35 The exchange-correlation energy was modeled using the generalized gradient approximation, as stated in the Perdew–Burke–Ernzerhof parametrization. 36 van der Waals interactions were included with empirical dispersion corrections (DFT-D3). 37 The electronic states were expanded in plane waves with an energy cutoff of 400 eV. A (2 × 2) surface unit cell was used, 4 atomic layers in thickness, with a 15 Å vacuum space added in

ACS Catalysis pubs.acs.org/acscatalysis Research Article

the z direction. The Brillouin zone integration was done using $5 \times 5 \times 1$ k-point grids.

The kinetic simulations were carried out by numerical integration of the rate equations, eqs 1–10 in Table 3, versus time, using an algorithm developed in house based on an Excel spreadsheet. The adjustable parameters, that is, the five equilibrium constants and four reaction rate constants, were optimized empirically to fit the experimental data, by minimizing the sum of the deviations between the experimental points from the kinetic runs and the values estimated by integration of the differential equations set. External information from other studies, such as the DFT calculations, was used to come up with initial educated guesses of these parameters but was not directly used to obtain their final values.

3. RESULTS

3.1. Catalysts Characterization. Several techniques and spectroscopies were used to characterize our catalysts. First, the actual metal loadings were measured by ICP-AES. The results from those measurements are contrasted with the nominal values in Table 1.

Representative images and NP size distribution data from the electron microscopy characterization of the catalysts are reported in Figure 1. The four panels on the left and center columns display typical STEM images and NP size distributions for Cu/SBA-15 (top, left), CuPt_{0.005}/SBA-15 (top, center), CuPt_{0.1}/SBA-15 (bottom, left), and Pt/SBA-15 (bottom, center). In all cases (but the pure Cu, see below), the small dark spots, corresponding to the metal NPs, are seen inside the 1D nanopores of the SBA-15 support, which were estimated by adsorption-desorption isothermal measurements to be about 7 nm in diameter; the average metal NP sizes were approximately 6.5 ± 2 nm in diameter, except for the case of the pure Cu catalyst, where the NPs were significantly larger $(\langle d \rangle = 24 \pm 6 \text{ nm})$; those were possibly located outside the pores. Although the diameters of the NPs and pores are close to each other, we saw no evidence for the reaction kinetics being controlled by mass transport: clear differences in kinetics were measured across the sequence of catalysts even though they all (bar the pure Cu one) have comparable NP sizes. The well-dispersed nature of the Pt atoms within the bimetallic NPs required for single-atom alloy (SAA) catalysis was checked by EDS, as exemplified in the image provided in the top, right panel of Figure 1.16 It should be noted that the EDS images do not offer sufficient resolution to determine if the Pt is disperse as single atoms or small clusters, though.

The crystallinity of the metal NPs was made evident by high-resolution TEM images such as that in the bottom right panel of Figure 1 and was confirmed independently by XRD. Representative data from the latter studies are reported in Figure 2. The XRD traces of all low-Pt-content samples, up to the CuPt_{0.01}/SBA-15 catalyst (at least), show diffraction peaks only for Cu. Moreover, the dimensions of the Cu unit cell do not appear to change significantly with the addition of (small amounts of) Pt. Another significant piece of information here is that the NP crystals are made out of metallic Cu. Previous XPS analysis of these catalysts have indicated the formation of a thin layer of copper oxide on the surface of the metal NPs, ¹⁶ but the XRD data clearly indicate that the bulk of those NPs still remains in the metallic state.

One key property of these catalysts in terms of their use to promote hydrogenation reactions is their ability to activate

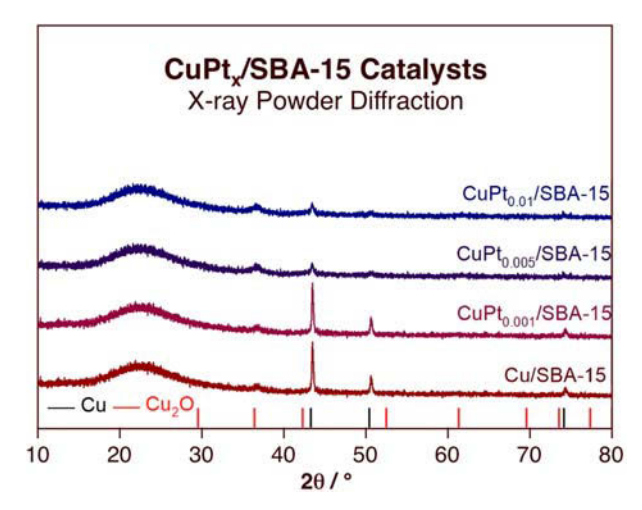


Figure 2. XRD data for selected $\text{CuPt}_{x}/\text{SBA-15}$ catalysts, indicating the crystallinity of the metal NPs. They are mainly metallic Cu crystals.

molecular hydrogen and promote reduction reactions. A comparative test of the reducing power of our catalysts was carried out by performing H_2 -TPR experiments. Typical data resulting from those studies are shown in Figure 3. It is clear

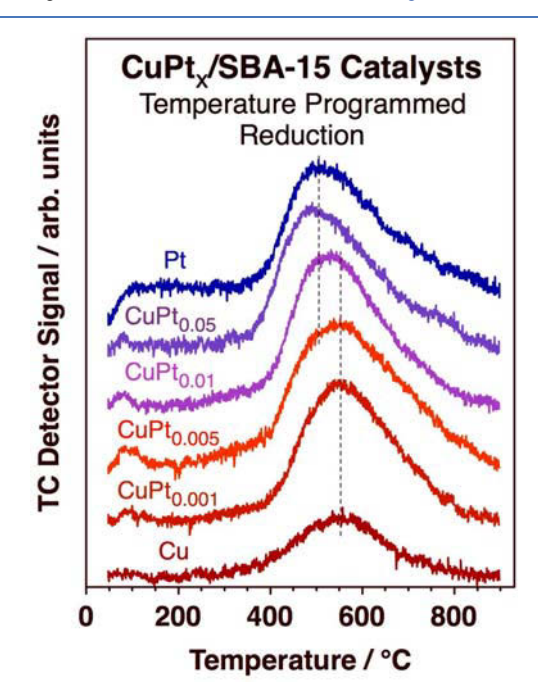


Figure 3. H₂-TPR traces for selected CuPt_x/SBA-15 catalysts.

from that figure that the temperature at which reduction can be promoted shifts to lower values with increasing Pt content: the $\rm H_2\text{-}TPR$ peak maximum shifts from an initial value of approximately 550 °C for the pure Cu/SBA-15 sample to about 490 °C for CuPt_{0.05}/SBA-15. This latter number is close to, perhaps even a bit lower than that for pure Pt/SBA-15 ($T_{\rm max}({\rm Pt}) \sim 520$ °C). It would appear that the addition of Pt facilitates the activation of $\rm H_2$, a behavior that is expected and the basis for the hypothesis that Pt needs to be added to Cu catalysts to enhance activity in hydrogenation reactions. In fact,

ACS Catalysis pubs.acs.org/acscatalysis Research Article

the total yield also increases upon the incorporation of even a small amount of Pt into the Cu NPs, another indication of the promoting effect of the added Pt. The H₂-TPR results may also help explain why the average NP size in the pure Cu/SBA-15 catalyst is so much larger than in all the other, Pt-containing, samples, as the Pt ions from the inorganic precursor used in the synthesis of the catalyst may be more easily reduced than those from the Cu salt and may produce more nucleation sites on the surface during the initial reduction step and also help with the reduction of the Cu ions.

3.2. Catalytic Performance. An initial assessment of the relative performance of our catalysts as a function of Pt content (x) was done by carrying out catalytic reactions for a set time (150 min) and then analyzing the reaction mixture in order to extract values for the total CMA conversion and for the selectivity toward CMO, HCMA, and 3-phenylpropanol (HCMO, also known as 1,2-dihydrocinnamyl alcohol) production. The results from runs using three different hydrogen pressures $(P(H_2) = 12.5, 25.0, \text{ and } 37.5 \text{ bar})$ are reported in Figure 4. Several observations are worth high-

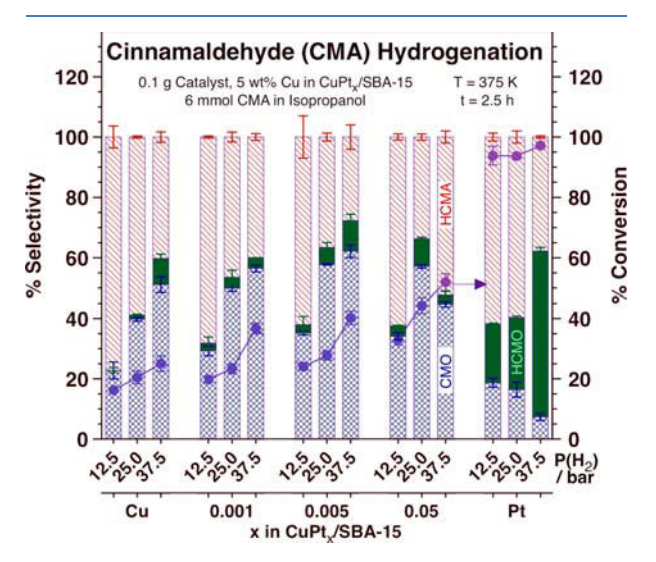


Figure 4. Total conversion and selectivities for CMO, HCMA, and HCMO production from the hydrogenation of CMA promoted by selected $\text{CuPt}_x/\text{SBA-15}$ catalysts ($x = 0, 0.001, 0.005, 0.05, \text{ and } \infty$). Data for runs carried out at three different H₂ pressures (12.5, 25.0, and 37.5 bar) are reported.

lighting from these data: (1) the total activity of the catalysts increases monotonically with both increasing Pt content and increasing $P(H_2)$, a result typical of hydrogenation reactions; ^{38,39} (2) the selectivity toward HCMA decreases with increasing $P(H_2)$, mainly at the expense of increases in CMO and HCMO production (presumably because the different adsorption geometries of the intermediates associated with each product require different local hydrogen surface coverages); ⁴⁰ (3) total hydrogenation to HCMO increases, in general, with both $P(H_2)$ and Pt content; and (4) critically, the selectivity for making CMO, the desirable product, peaks with catalysts with low Pt content, that is, for $x \sim 0.005$. These trends will be discussed in more detail below.

Additional kinetic data are provided in Figure 5, in the form of total turnover frequencies (TOFs) and selectivities (calculated on the basis of the individual TOFs for each product relative to the total TOFs, stacked to add to a total of

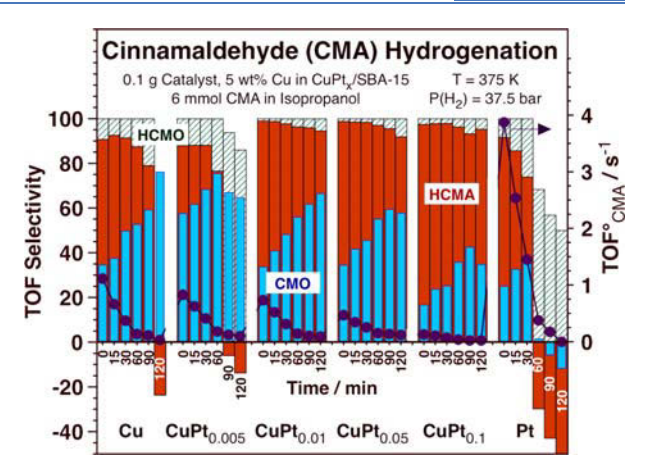


Figure 5. Total TOFs and selectivities in terms of the TOFs of production of the individual products (CMO, HCMA, and HCMO) as a function of time for the hydrogenation of CMA promoted by selected $\text{CuPt}_x/\text{SBA-15}$ catalysts ($x = 0, 0.005, 0.01, 0.05, 0.01, \text{ and } \infty$).

100%) versus reaction time. In all cases the rates decrease rapidly after a few minutes of reaction, but the effect seems to be more pronounced with the catalysts with the most Cu content (the TOF with Pt/SBA-15 also decreases rapidly, but that is because about 85% conversion is reached already after 30 min of reaction). Also, the production of HCMO appears to become important only after significant accumulations of CMO and HCMA in the reaction mixture, suggesting that the direct hydrogenation of CMA to HCMO⁴⁰ is negligible and that HCMO is mainly a secondary product. On the other hand, in some cases the net concentrations of the primary products, CMO and, particularly, HCMA, decrease at the later stages of the reaction, because their rate of consumption to yield HCMO is higher than their rate of production from CMA; this is indicated in Figure 5 by the negative values reported for their TOF selectivities.

Next, the initial TOF appears to go down as Pt is added to the Cu catalysts. However, this observation needs to be interpreted with some caution, because part of the reason why the TOF with pure Cu is high is because those NPs are larger than the rest (larger NPs expose less atoms on the surface, so the total conversion is normalized to a smaller number of assumed catalytic sites). Moreover, it is not clear what the active sites for the hydrogenation reaction may be (Pt, Cu, Pt + Cu, etc.); the total number of surface atoms in the metal NPs was used in our TOF calculations (as indicated in the Experimental Section), even if that may not be the appropriate parameter for the normalization of conversions to TOFs. As indicated above, this issue does not affect the relative comparisons of selectivity, though. In terms of conversion versus time, the CuPt_{0.005}/SBA-15 is the Cu-containing catalyst that displays the faster total reaction rate (the Pt/SBA-15 catalyst is the most active overall). Finally, the relative TOFs for CMO increase in all cases as the reaction proceeds, compared to the rates of formation of the other products. As already indicated by the data in Figure 4, the best CMO selectivities were seen with the CuPt_{0.005}/SBA-15 catalyst.

The fast decrease in conversion rate with increasing reaction time mentioned above is better illustrated by plotting the TOFs as a function of the concentration of the initial reactant ([CMA]), in a log—log plot to extract apparent reaction kinetic

orders with respect to [CMA]. This has been done in Figure 6. The slopes extracted from these plots vary from m = 0.85 for

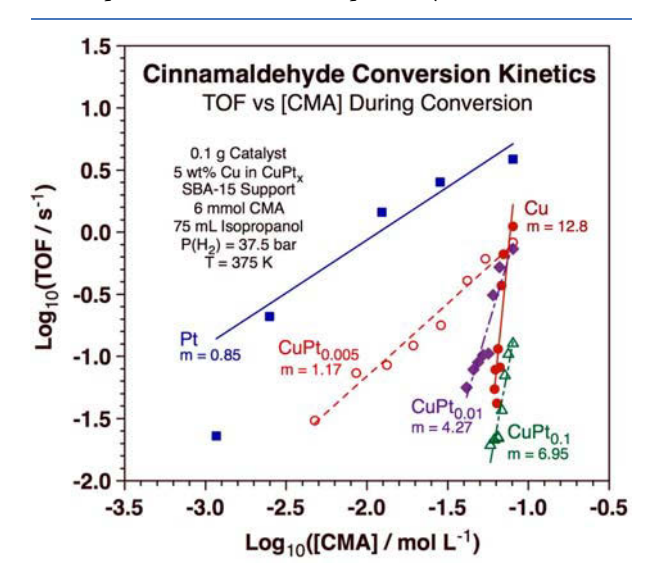


Figure 6. Log—log plot of TOFs versus [CMA] for the hydrogenation of CMA promoted by selected $\text{CuPt}_x/\text{SBA-15}$ catalysts ($x = 0, 0.005, 0.01, 0.1, \text{ and } \infty$).

the pure Pt catalyst to m = 12.8 for the pure Cu catalyst, with intermediate and increasing values as the Pt content in the $CuPt_x/SBA-15$ samples is decreased. The kinetic reaction orders implied by this analysis are unreasonably high and indicate that additional factors, besides the reaction rate dependence on [CMA], play a role in determining reaction rates. Two possibilities are considered in the following analysis: (1) the surface of the catalysts, primarily the Cu atoms, are

poisoned by organic deposits that form and bind strongly on the surface during the course of the reaction, a common occurrence in hydrogenation catalysis; 41–44 and/or (2) the products of the reaction, CMO, HCMA, and HCMO, may compete for adsorption sites on the surface, blocking the CMA uptake and consequently inhibiting further catalytic activity.

A more careful kinetic study was carried out by performing catalytic runs systematically versus $P(H_2)$ and [CMA] to extract reaction-rate orders. The results are summarized in Figure 7 and Table 2 (reaction rate orders were calculated

Table 2. Kinetic Reaction-Rate Orders with Respect to $P(H_2)$ for the Hydrogenation of CMA to CMO and HCMA on $CuPt_x/SBA-15$ Catalysts

$n(H_2)$	Cu/SBA-15	CuPt _x /SBA-15	Pt/SBA-15
CMA consumption	0.4	0.5 ± 0.1	0.0
CMO production	1.1	0.9 ± 0.2	-0.8
HCMA production	-0.2	0.0 ± 0.3	-0.4

directly from the slope of the linear fits to the data in Figure 7). In terms of the dependence of the conversion on $P(H_2)$ (Figure 7, top row, and Table 2), a positive kinetic reaction rate order is seen with most $CuPt_x/SBA-15$ catalysts, especially in connection with the production of CMO (second panel from the right), for which the kinetics is approximately first order; the order is close to zero for HCMA, for an average of half order for the total consumption of CMA. A few conclusions can be derived from these numbers. First, the detectable dependence of the conversion rates on $P(H_2)$ indicates that the coverage of hydrogen atoms on the surface is low. Moreover, the half-order seen for the total conversion of CMA on $P(H_2)$ can be associated with a linear dependence of the rates on atomic-hydrogen coverage (at low coverages), suggesting that the rate-limiting step is the incorporation of the

Cinnamaldehyde TONs vs P(H₂) & [CMA]°

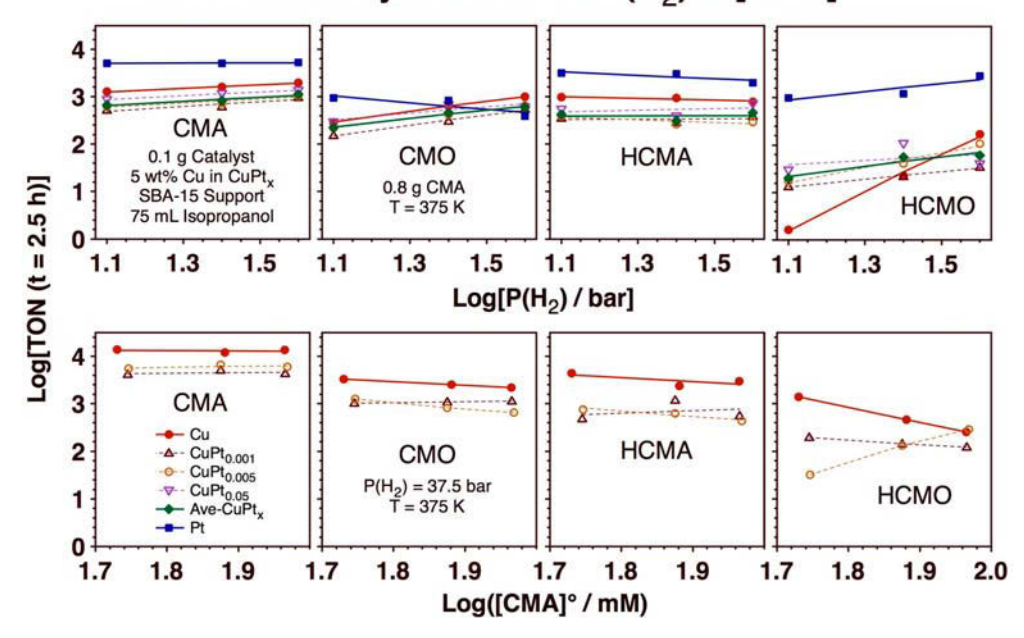


Figure 7. Log-log plots of the TONs after 150 min (2.5 h) of reaction for the hydrogenation of CMA promoted by selected $CuPt_x/SBA-15$ catalysts ($x = 0, 0.001, 0.005, 0.01, and \infty$) versus $P(H_2)$ (top row) and CMA (bottom).

Cinnamaldehyde Hydrogenation Kinetics

Catalyst Recycling Tests

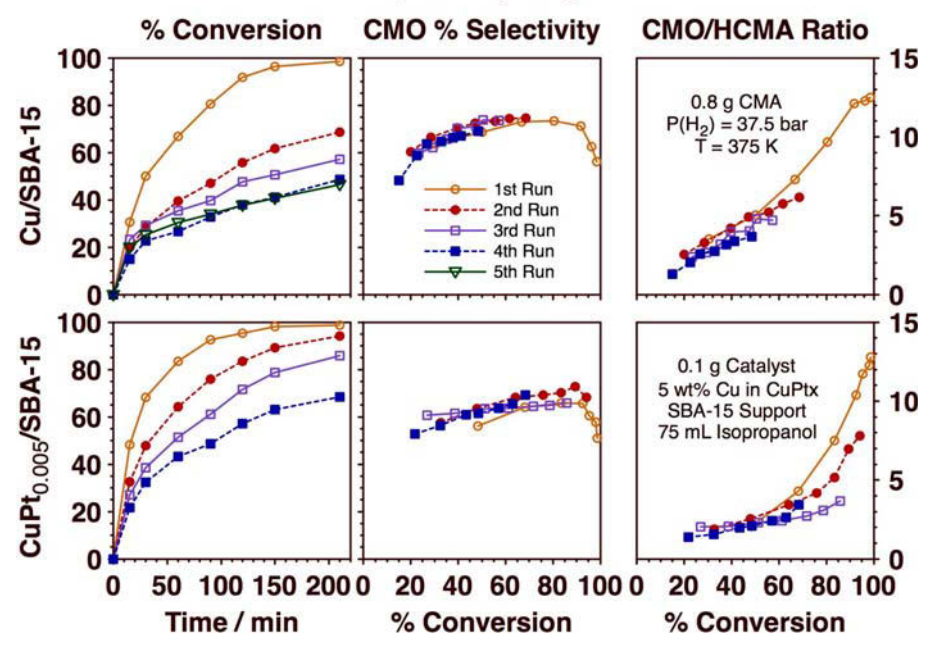


Figure 8. Kinetic data in the form of total CMA conversion versus reaction time (left), and CMO% selectivity (center) and CMO/HCMA ratio (right), both versus total conversion, for the hydrogenation of CMA promoted by Cu/SBA-15 (top row) and CuPt_{0.005}/SBA-15 (bottom). The traces in each panel correspond to results obtained with the same catalyst after recycling without any pretreatments in between catalytic runs.

first hydrogen atom into the adsorbed CMA, as it is in many other hydrogenation reactions. $^{18,38-40,45-57}$ This interpretation is a simplification, as additional subtleties are associated with the differences in reaction rate orders seen for CMO versus HCMA: it would seem that CMO production is much more sensitive to $\theta_{\rm H}$ than HCMA formation (as already mentioned and explained above). In any case, it is interesting to note that none of the $P(H_2)$ reaction-rate orders changes significantly upon the addition of Pt to the Cu-based catalysts. The exception here is the case of HCMO production, for which a much stronger (positive) dependence is seen with pure Cu, perhaps an indication of the difficulty for activating H_2 on that metal.

By contrast, the estimated $P(H_2)$ orders for the production of both CMO and HCMA on the pure Pt catalyst appear to be negative. However, this is likely to be an artifact, because the TONs were calculated after 2.5 h of reaction, at which point significant further hydrogenation of CMO and HCMA to HCMO takes place. More reliable is the $P(H_2)$ order estimated for the overall consumption of CMA, which is close to zero. In this case, the surface is likely to be saturated with atomic hydrogen, possibly because Pt is a good promoter of the dissociative adsorption of H_2 .

In terms of the kinetic reaction rate orders for the consumption of CMA or for the production of either CMO or HCMA with respect to the concentration of CMA in solution, they are all close to zero (within the large uncertainties of the measurements; Figure 7, bottom row). This suggests that the surface is nearly saturated with adsorbed hydrocarbons under reaction conditions. Certainly, no strong dependences of the sort seen in Figure 6 are observed here; the

behavior reported in Figure 6 must be ascribed to factors other than the kinetic rate law of the reaction.

The possibility that the surface of these catalysts may become poisoned by the adsorption of strongly bonded hydrocarbon residues was tested by carrying out sequential CMA conversion runs with the same catalyst without any conditioning in between. Examples of the results obtained from those studies are shown in Figure 8. It is seen there that, indeed, the catalysts loose some activity after being used several times. However, this effect is not very pronounced: the initial activity of both Cu/SBA-15 and CuPt_{0.005}/SBA-15 catalysts goes down only by about a factor of 2 after being used five consecutive times, and that is in great measure the result of the loss of some catalyst powder during the filtering process used to separate the catalyst from the solution between catalytic runs (a total loss of about 40% after the five runs). The potential mild poisoning indicated by the data in Figure 8 cannot account for the large apparent reaction-rate orders in [CMA] implied by the analysis of the data in Figure 6. Moreover, the behavior of these catalysts in terms of selectivity toward the production of CMO, expressed either as a % selectivity (Figure 8, center panels) or in terms of CMO/ HCMA ratios (right), does not change significantly from run to run. Interestingly, a clear increase in CMO selectivity with extent of conversion is seen here in all cases, for all catalytic runs, and the return to lower selectivities every time as the new reactions are started is also evident.

The main conclusion from all these tests is that the changes in the catalytic performance of the $CuPt_x/SBA-15$ catalysts with reaction time cannot be fully explained by poisoning of the surface. Instead, we favor the idea that the kinetic changes are a consequence of the preferred adsorption of the products

ACS Catalysis pubs.acs.org/acscatalysis Research Article

in the presence of the reactant as they accumulate in the liquid mixture (although poisoning may also play a part). To get a better idea of the kinetics of the side steps involved in the overall process, the further hydrogenation of CMO and HCMA to HCMO was tested independently; the kinetics of those conversions on Cu/SBA-15, CuPt_{0.005}/SBA-15, and Pt/SBA-15 are shown in Figure 9. In all cases it was found that Pt

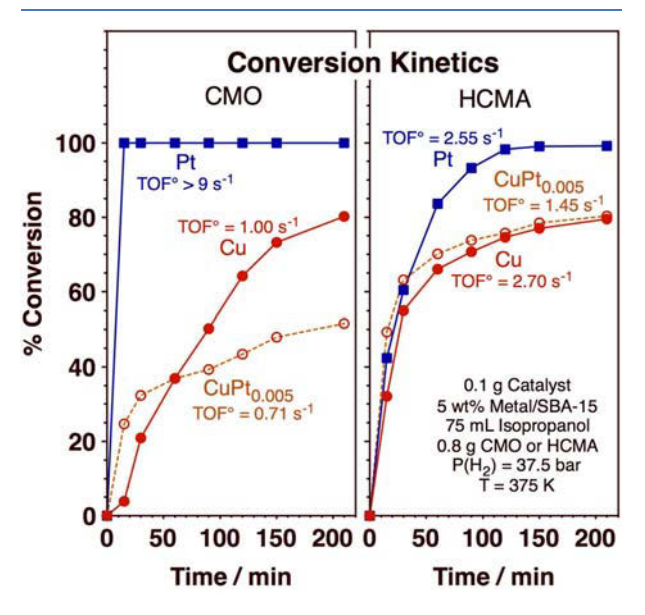


Figure 9. % conversion versus time for the hydrogenation of CMO (left panel) and HCMA (right) promoted by Cu/SBA-15, CuPt_{0.005}/SBA-15, and Pt/SBA-15 catalysts.

is the most active hydrogenation catalyst. In relative terms, Pt/ SBA-15 promotes the hydrogenation of CMO at a faster rate than the hydrogenation of HCMA. With pure Cu catalysts the two rates are closer, but the ordering gets reversed: HCMA is hydrogenated faster than CMO. Pt-containing Cu catalysts (CuPt_{0.005}/SBA-15 in the example reported in Figure 9) seem to retain the same activity of pure Cu for the hydrogenation of HCMA but may lose some activity in the case of CMO. One general observation of relevance to the hydrogenation of CMA is that all the TOFs in Figure 9 are relatively high, about 1 s⁻¹ or higher. These values are comparable to those measured for the hydrogenation of CMA (Figure 5), which means that the slow conversion of the products from CMA (CMO and HCMA) to HCMO with all of our catalysts bar the pure Pt one must be because of the limited access of the primary products, CMO in particular, to the surface.

The relative adsorption energies of the reactant and of the primary products were estimated by DFT calculations. The results are reported in Figure 10, for crotonaldehyde (CTA) instead of CMA to make the calculation a bit simpler; the trends are expected to be the same. It is seen there that, on pure Cu, the adsorption of the reactant (CTA) is much weaker than that of the products: the energies of adsorbed crotyl alcohol (CTO) and of adsorbed butanal (HCTA) are 23 and 69 kJ/mol lower, respectively (referenced to CTA(ads) + 2 H(ads)). These calculations were performed by adding two molecules to the Cu unit cell, to emulate the high total hydrocarbon coverages implied by the weak kinetic dependence of the reaction rates on the concentration of the unsaturated aldehyde (Figure 7). The energetics of mixed

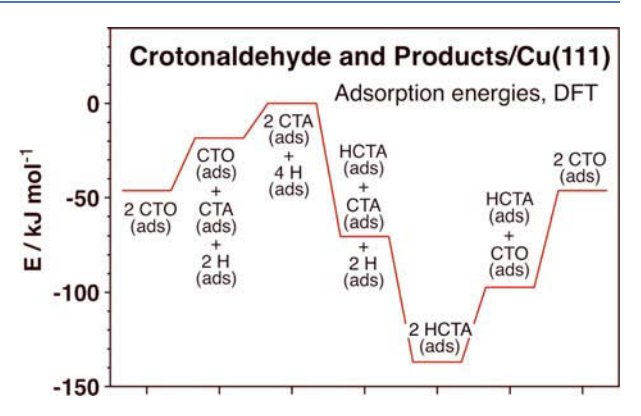


Figure 10. DFT calculations of the energies of adsorption for crotonaldehyde (CTA) and its primary hydrogenation products crotyl alcohol (CTO) and butanal (HCTA), all referenced to CTA adsorbed on a H-covered Cu(111) surface.

layers was calculated as well, but no significant synergies were identified: the adsorption energies of the mixtures are quite close to those estimated by simple addition of the individual adsorbates. This suggests that the competitive adsorption of all of the organic molecules can be described by a simple set of Langmuir isotherms (see below).

All the kinetic information acquired in the experiments reported above was put together to propose a simple microkinetic mechanism for the hydrogenation of CMA on the CuPt_x/SBA-15 catalysts. A couple of approximations were incorporated in this model: (1) the adsorption of all the organic molecules (CMA, CMO, HCMA, and HCMO) was described by Langmuir isotherms for competitive reversible adsorption in equilibrium and in the high-coverage limit; and (2) the dissociative adsorption of molecular hydrogen was also described by a Langmuir isotherm at equilibrium, albeit in the low-coverage limit (as the reaction-rate orders are far from zero, Figure 7 and Table 2). It should be indicated that this latter approximation was in fact not required in our calculations, because the kinetic data used were all obtained for a fixed value of P(H₂), 37.5 bar, which represents a large excess, and because we assume that the coverage of atomic hydrogen on the surface, whatever its value, remains constant throughout the progress of the reactions; here we only report pseudo rate constants, which include the hydrogen coverage term.

Another approximation in this model is that all the catalytic sites are treated as equal. The rationale for this choice is that the conversion of the reactant (the unsaturated aldehyde) is expected to occur on specific selective sites, presumably on the Cu surface. Hydrogenation to the different products takes place stepwise, but it is assumed to all happen on the same initial adsorption site. In terms of the role of hydrogen, it is assumed that even if the activation of H_2 takes place on separate and different catalytic sites, the resulting adsorbed H atoms then spillover and diffuse to the sites where the hydrocarbon reactants are bound and converted.

The proposed mechanism consists of the steps in Table 3. All the hydrogenation steps, eqs 7-10 in Table 3, are considered irreversible and far from equilibrium.

Examples of the fits of this model to our experimental results are presented in Figure 11. The left three panels show the data from the catalytic runs obtained with (from left to right) Cu/SBA-15, CuPt_{0.005}/SBA-15, and Pt/SBA-15, in the form of

Table 3. Proposed Mechanism for Hydrogenation

$$CMA(sol) \leftrightarrow CMA(ads) \qquad \theta_{CMA} = \frac{K_{CMA}[CMA]}{1 + \sum K_c[c]} \qquad (1)$$

$$CMO(sol) \leftrightarrow CMO(ads) \qquad \theta_{CMO} = \frac{K_{CMO}[CMO]}{1 + \sum K_c[c]} \qquad (2)$$

$$HCMA(sol) \leftrightarrow HCMA(ads) \qquad \theta_{HCMA} = \frac{K_{HCMA}[HCMA]}{1 + \sum K_c[c]} \qquad (3)$$

$$HCMO(sol) \leftrightarrow HCMO(ads) \qquad \theta_{HCMO} = \frac{K_{HCMO}[HCMO]}{1 + \sum K_c[c]} \qquad (4)$$

$$\sum K_c[c] = K_{CMA}[CMA] + K_{CMO}[CMO] + K_{HCMA}[HCMA] + K_{HCMO}[HCMO] \qquad (5)$$

$$H_2(g) \leftrightarrow 2 \text{ H(ads)} \qquad \theta_H = K_{H_2}^{1/2} p_{H_2}^{1/2} \qquad (6)$$

$$CMA(ads) + 2 \text{ H(ads)} \leftrightarrow CMO(ads) \qquad R_{CMO} = (k_{CMO} \theta_H^{n_{CMO}}) \theta_{CMA} = k'_{HCMO} \theta_{CMA} \qquad (7)$$

$$CMA(ads) + 2 \text{ H(ads)} \leftrightarrow HCMA(ads) \qquad R_{HCMA} = (k_{HCMA} \theta_H^{n_{HCMO}}) \theta_{CMA} = k'_{HCMA} \theta_{CMA} \qquad (8)$$

$$CMO(ads) + 2 \text{ H(ads)} \leftrightarrow HCMO(ads) \qquad R_{HCMO2} = (k_{HCMO2} \theta_H^{n_{HCMO2}}) \theta_{CMO} = k'_{HCMO2} \theta_{CMO} \qquad (9)$$

$$HCMA(ads) + 2 \text{ H(ads)} \leftrightarrow HCMO(ads) \qquad R_{HCMO1} = (k_{HCMO1} \theta_H^{n_{HCMO2}}) \theta_{HCMA} = k'_{HCMO2} \theta_{HCMA} = k'_{HCMO1} \theta_{HCMA} \qquad (10)$$

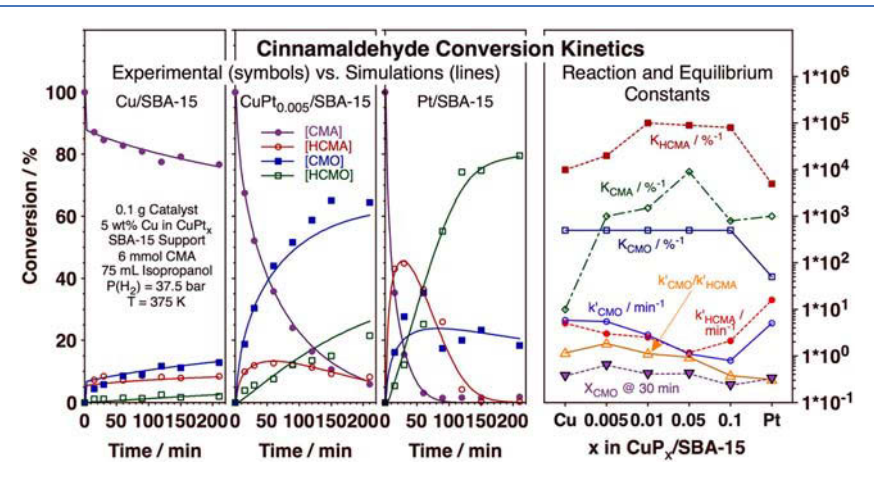


Figure 11. Kinetics of the hydrogenation of CMA on $CuPt_x/SBA-15$ catalysts. Left three panels: % CMA conversion and % HCMA, CMO, and HCMO yields versus reaction time for runs carried out using Cu/SBA-15 (left), $CuPt_{0.005}/SBA-15$ (center), and Pt/SBA-15 (right). The symbols correspond to the experimental data, whereas the lines are the result of our microkinetic simulations (see text). Far right: Kinetic parameters extracted from the microkinetic simulations, plotted versus Pt content.

conversions and yields versus reaction time, whereas the farright panel reports the values obtained for the key reaction and equilibrium constants from our fits. At first sight it may seem that there are a large number of parameters to fit to the data, but in reality those could be reduced to only a few. First, the orders of the reactions with respect to the $\rm H_2$ pressure were measured experimentally (Table 2) and in the end incorporated, together with $\rm K_{H2}$, into pseudo reaction rate constants (taking advantage of the fact that the hydrogen pressure is high and constant in all cases, as mentioned above). Second, the reaction and equilibrium constants associated with the secondary hydrogenation of the primary products (HCMA and CMO) to HCMO are only relevant toward the end of the

reaction, if at all; we did fit those parameters as well, but do not report them as they do not provide much additional information. Only the equilibrium constants for CMA, HCMA, and CMO and the pseudo rate constants for steps 7 and 8 needed to be adjusted, and even in those there are some correlations that made a few of the values not critical to the fits. The final values for $K_{\rm CMA}$, $K_{\rm HCMA}$, $K_{\rm CMO}$, $k'_{\rm HCMA}$, and $k'_{\rm CMO}$ obtained from these fits are reported as a function of catalyst composition in the far right panel of Figure 11, together with the $k'_{\rm CMO}/k'_{\rm HCMA}$ ratio and the molar fraction of CMO ($X_{\rm CMO}$).

Some interesting trends can be identified from those data. First, it is worth noticing that the equilibrium constant for

CMA adsorption is anomalously low on the pure Cu catalyst. This was expected based on the energetics calculated by DFT (Figure 10), but the observation is unique to the Cu/SBA-15 case (it is not seen with any of the other catalysts) and explains why the reaction with Cu slows down so dramatically early on in the catalytic runs (Figure 6): both HCMA and CMO compete favorably with CMA for Cu sites and poison the catalytic sites as soon as a minor concentration of the products builds up in the reaction mixture, within 2-3 min. Indeed, our calculations of surface coverages deriving from the kinetic simulation yielded a CMA coverage of $\theta_{\rm CMA} \sim 0.98$ ML after 1 min of reaction but values of $\theta_{\rm CMA} \sim 0.05$ ML—and $\theta_{\rm HCMA}$ + $\theta_{\rm CMO}$ > 0.95 ML—after 3 min (the full time evolution of all surface coverages is provided in the Supporting Information). Also, in all cases with bimetallic NPs, HCMA adsorbs more strongly than CMO and therefore dominates in term of surface coverages, although the effect seems to be the most accentuated with the catalysts with intermediate Pt loads. Our calculations of surface coverages from the kinetic simulations indicate almost complete saturation with the products of the hydrogenation reaction ($\theta_{HCMA} + \theta_{HCMO} > 0.8$ ML in most cases) after \sim 10 min from the start of the reaction. A full account of the time dependence of these coverages is provided in the Supporting Information.

In terms of reaction rate constants, the Pt catalyst is significantly more active than any of the Cu containing ones for all hydrogenation steps, but it is also more active for the production of HCMA versus CMO in relative terms, which is the reason why it exhibits such a poor selectivity toward the making of the desirable CMO. Interestingly, the rate constants also decrease monotonically when starting with Cu as the Pt content is increased; the main reason why Cu exhibits slower conversion is that the surface coverage of adsorbed CMA is particularly low in that case, as mentioned before. It should be said that the decrease in the values of both reaction rates, k'_{HCMA} and k'_{CMO} , with Pt content (x) is significantly more pronounced than what would be expected based on pure geometrical (site-blocking) arguments: there is a clear synergy between the two metals that makes Pt affect the reactivity of the Cu surface sites in the alloys.

Finally, selectivity toward the production of CMO, displayed in Figure 11 as the molar fraction of CMO made (relative to all the products, $X_{\rm CMO}$) after 30 min of reaction (purple, downward-pointing triangles) correlates nicely with the ${k'}_{\rm CMO}/{k'}_{\rm HCMA}$ ratio (orange trace, upward-pointing triangles). This is clearly the parameter that controls selectivity, and that is modified by changes in the composition of the bimetallic nanoparticles. It should be remembered that these pseudo reaction rate constants do include the contribution from the coverage of atomic hydrogen on the surface, but, as discussed above, the dependence of the rates of both CMO and HCMA production on P(H₂) should not change with the Pt content in the catalysts. Moreover, if anything, selectivity toward CMO production increases with increasing $P(H_2)$ (Figures 4 and 7), which means that if the addition of Pt facilitates H2 dissociative adsorption on the surface and consequently leads to an increase in the coverage of atomic H, that factor should induce an increase in the value of $k'_{\rm CMO}$ with respect to $k'_{\rm HCMA}$ with increasing Pt content: the opposite is the case here. We believe that the trend for k'_{CMO}/k'_{HCMA} reported in Figure 11 reflects an intrinsic change in the rates of the incorporation of the first H in the adsorbed CMA, which is presumed to occur on Cu sites. It appears that the addition of Pt to the Cu-based catalysts may not only facilitate the uptake of H₂ but also modify the reactivity of the Cu surface.

4. DISCUSSION AND CONCLUSIONS

Here, we have reported results from a comprehensive kinetic study of the hydrogenation of cinnamaldehyde (CMA) promoted by catalysts comprised of Cu–Pt alloys dispersed on a mesoporous (SBA-15) support. The kinetic measurements were carried out as a function of the composition of the metallic NPs with the aim of identifying synergies leading to better catalytic performance in terms of selectivity toward the desired product, the unsaturated alcohol (cinnamyl alcohol in this case, CMO). A total of 10 catalysts were made, pure Cu/SBA-15 and Pt/SBA-15 and another eight CuPt_x/SBA-15 compositions with x varying from 0.001 to 0.75, as corroborated experimentally by ICP-AES (Table 1).

Our studies were initiated by a careful characterization of the catalysts to ensure that they all exhibit similar properties except for the Pt-to-Cu ratio. TEM images (Figure 1) indicated that the average NP size was approximately 6.5 nm in all cases except for the pure Cu/SBA-15 catalyst, which exhibit larger NPs, perhaps because the Cu ions are more difficult to reduce than those of Pt and therefore form less nucleation sites on the surface. In addition, both TEM (Figure 1) and XRD (Figure 2) data pointed to the formation of Cu crystalline phases in all cases but with the pure Pt/SBA-15. The Pt atoms in the diluted CuPt_x/SBA-15 bimetallic NPs were found to be finely dispersed, likely in atomic form, as indicated by EDS imaging (Figure 1). The increase in ease of reducibility with increasing Pt content, a property believed to facilitate catalytic hydrogenation reactions, was established by H_2 -TPR (Figure 3).

Kinetic catalytic studies corroborated that small amounts of Pt improve the performance of the Cu catalysts: optimum selectivity toward the desired CMO was observed with the CuPt_{0.005}/SBA-15 catalyst (Figure 4). This confirms previous reports by us 16 and others 12 ,13,58,59 on the beneficial effect of adding small amounts of a second metal (Pt) to the first (Cu) to improve hydrogenation catalysis. The working hypothesis to explain the selectivity enhancement observed with these so-called single-atom alloy (SAA) catalysts has been that the majority metal, Cu in this case, is chosen because of its desirable catalytic properties, a preference for C=O hydrogenation steps in the presence of C=C bonds, but needs to be complemented with a second metal (Pt) to perform the first step in these reactions, the activation of $\rm H_2$. 20,58

As discussed in the Introduction, that hypothesis has been supported by extensive and elegant experiments with model single crystals under ultrahigh vacuum conditions, mainly by the group of Sykes and co-workers at Tufts University, ⁵⁸ but has been recently challenged by us on the account that the Pt atoms in these catalysts may not be present on the surface under reaction conditions but rather placed underneath a thin copper oxide layer that forms on top. ¹⁶ The possible dynamic diffusion of the metals in these bimetallic NPs under realistic reaction conditions complicates the picture and calls into question the model used so far to explain the selectivity enhancement obtained with SAAs catalysts.

Analysis of the kinetic data from the studies reported here points to some synergies between the metals that may offer an alternative view of the source of the increase in hydrogenation selectivity observed. Critically, in batch reactors such as that used here, the catalytic activity dies down rather quickly, in a particularly dramatic way with the pure Cu/SBA-15 catalyst

(Figure 5 and 6), and the selectivity toward the unsaturated alcohol (CMO) increases with the extent of the reaction (Figure 5). Unreasonably large kinetic reaction rate orders with respect to the concentration of the reactant ([CMA]) are obtained from analysis of the time-dependent kinetic data (Figure 6), not matched by the more reasonable values estimated using an initial-rate method (Figure 7). It could be argued that the rapid activity loss seen in these reactions may be due to poisoning of the surface with strongly adsorbed carbonaceous deposits, a phenomenon typical of many hydrogenation catalytic systems, ⁴³ but that idea was disproved here by the fact that most of the activity is recovered upon changing the spent reaction mixture with a fresh one (Figure 8).

Instead, our explanation is that activity and selectivity are affected, at least in part, by the competition among the reactant (CMA) and the products (CMO, HCMA, HCMO) for adsorption sites on the surface. DFT calculations highlighted the particularly weak nature of the bonding of the unsaturated aldehyde on pure Cu surfaces relative to either the unsaturated alcohol or the saturated aldehyde, with the latter being the one that dominates the adsorption (Figure 10). The further hydrogenation of either CMO or HCMA to HCMO also depends strongly on the composition of the bimetallic NPs (Figure 9). All the experimental kinetic data acquired in this study were put together into a simple microkinetic model where the organic molecules saturate the surface following Langmuirian competitive adsorption equilibria, where H₂ adsorbs dissociatively in separate sites to produce small coverages of adsorbed hydrogen atoms and where the adsorbed reactants then undergo stepwise hydrogenation to yield both CMO and HCMA primary products and then the secondary HCMO product (eqs 1-10, Table 3).

Our microkinetic model explains most of the kinetic trends observed as a function of NP metal composition. As mentioned above, the rapid decrease in conversion rates seen at the start of the catalytic runs can be explained by site poisoning via the adsorption of the products, HCMA in particular (Figure 11). 0.1), the adsorption equilibrium constant for HCMA was estimated to be approximately 200 larger than that for CMO, and in most cases ~1000 larger than that for CMA (with the exception of the x = 0.05 case). On the other hand, reaction selectivities were found to be defined mainly by the relative values of the rate constants of the initial hydrogenation steps. In this case Pt is unique in that it not only displays reaction rate constants up to an order of magnitude larger than those of the other (Cu-containing) catalysts, but also because the rate constant for HCMA formation is 3 to 4 times larger than that for CMO production; this explain why Pt shows such poor selectivity toward CMO in this process. With the alloys, both rate constants decrease with decreasing Pt content up to $x \sim$ 0.05-0.1, after which they go up all the way to the case of the pure Cu/SBA-15. More importantly, the $k'_{\rm CMO}/k'_{\rm HCMA}$ ratio reaches a maximum at x = 0.005, the same metal composition for which the best selectivity for CMO production was observed. It appears that it is the intrinsic activity of the hydrogenation sites, most likely on the Cu surface, which controls the performance of the catalyst.

In more general terms, it is important to note that the values of all of the equilibrium and kinetic constants vary significantly, usually by an order of magnitude, with the value of x in the CuPt, bimetallic nanoparticles. This indicates that perhaps the

individual Pt atoms added to the Cu NPs cannot be viewed simply as isolated atoms that retain their own chemical properties, but rather as elements that affect the collective electronic structure of the whole NPs, or at least an ensemble of Cu atoms around it. In fact, this is the view taken historically when describing alloys, ⁶⁰ and it is still one used nowadays to describe and optimize catalytic performance. ^{61–63} Optimization of the performance of SAA catalysts clearly depends on other factors besides the increased activation of H₂ presumably provided by the added Pt. It should also be said that the effect of the added Pt may be somewhat localized, but perhaps not at an atomic scale; even if the Pt atoms are present at the subsurface of the metal NPs, they can still exert an effect on the chemical behavior of the surface. Either way, determining the exact location of these Pt atoms under reaction conditions requires the characterization of the catalysts in situ as the hydrogenation reactions take place.

ASSOCIATED CONTENT

Solution Supporting Information

The Supporting Information is available free of charge at https://pubs.acs.org/doi/10.1021/acscatal.9b05407.

Time dependence of the surface coverages of the adsorbed organic reactants and products, as calculated using our microkinetic model (PDF)

AUTHOR INFORMATION

Corresponding Author

Francisco Zaera — Department of Chemistry and UCR Center for Catalysis, University of California, Riverside, California 92521, United States; orcid.org/0000-0002-0128-7221; Email: zaera@ucr.edu

Authors

Yueqiang Cao — Department of Chemistry and UCR Center for Catalysis, University of California, Riverside, California 92521, United States; State Key Laboratory of Chemical Engineering, East China University of Science and Technology, Shanghai 200237, China; orcid.org/0000-0002-1036-4049

Jonathan Guerrero-Sańchez – Centro de Nanociencias y Nanotecnología, Universidad Nacional Autónoma de México, Ensenada, Baja California 22800, México

Ilkeun Lee – Department of Chemistry and UCR Center for Catalysis, University of California, Riverside, California 92521, United States

Xinggui Zhou — State Key Laboratory of Chemical Engineering, East China University of Science and Technology, Shanghai 200237, China

Noboru Takeuchi — Department of Chemistry and UCR Center for Catalysis, University of California, Riverside, California 92521, United States; Centro de Nanociencias y Nanotecnología, Universidad Nacional Autónoma de Mexico, Ensenada, Baja California 22800, Mexico

Complete contact information is available at: https://pubs.acs.org/10.1021/acscatal.9b05407

Notes

The authors declare no competing financial interest.

■ ACKNOWLEDGMENTS

Financial support for this project was provided by a grant from the U.S. National Science Foundation, Division of Chemistry (NSF-CHE 1660433). Y.C. acknowledges the 111 project of China (Grant No. B08021, Ministry of Education of the People's Republic of China and State Administration of Foreign Experts Affairs of People's Republic of China) for traveling support for his visit to Riverside to perform the reported experiments. N.T. and J.G.S. thank DGAPA-UNAM project IN100516, DGAPAUNAM project IN101019, and Conacyt grant A1-S-9070 for partial financial support. N.T. thanks DGAPA-UNAM for a scholarship at the University of California, Riverside. Calculations were performed in the DGCTIC-UNAM Supercomputing Center, project LANCAD-UNAM-DGTIC-051.

REFERENCES

- (1) Yang, X.-F.; Wang, A.; Qiao, B.; Li, J.; Liu, J.; Zhang, T. Single-Atom Catalysts: A New Frontier in Heterogeneous Catalysis. *Acc. Chem. Res.* **2013**, *46*, 1740–1748.
- (2) Pelletier, J. D. A.; Basset, J.-M. Catalysis by Design: Well-Defined Single-Site Heterogeneous Catalysts. *Acc. Chem. Res.* **2016**, *49*, 664–677
- (3) Gates, B. C.; Flytzani-Stephanopoulos, M.; Dixon, D. A.; Katz, A. Atomically Dispersed Supported Metal Catalysts: Perspectives and Suggestions for Future Research. *Catal. Sci. Technol.* **2017**, *7*, 4259–4275.
- (4) Liu, J. Catalysis by Supported Single Metal Atoms. ACS Catal. 2017, 7, 34–59.
- (5) Wang, A.; Li, J.; Zhang, T. Heterogeneous Single-Atom Catalysis. *Nat. Rev. Chem.* **2018**, *2*, 65–81.
- (6) Chen, Y.; Ji, S.; Chen, C.; Peng, Q.; Wang, D.; Li, Y. Single-Atom Catalysts: Synthetic Strategies and Electrochemical Applications. *Joule* 2018, 2, 1242–1264.
- (7) DeRita, L.; Resasco, J.; Dai, S.; Boubnov, A.; Thang, H. V.; Hoffman, A. S.; Ro, I.; Graham, G. W.; Bare, S. R.; Pacchioni, G.; Pan, X.; Christopher, P. Structural Evolution of Atomically Dispersed Pt Catalysts Dictates Reactivity. *Nat. Mater.* **2019**, *18*, 746–751.
- (8) Marcinkowski, M. D.; Liu, J.; Murphy, C. J.; Liriano, M. L.; Wasio, N. A.; Lucci, F. R.; Flytzani-Stephanopoulos, M.; Sykes, E. C. H. Selective Formic Acid Dehydrogenation on Pt-Cu Single-Atom Alloys. *ACS Catal.* **2017**, *7*, 413–420.
- (9) Marcinkowski, M. D.; Darby, M. T.; Liu, J.; Wimble, J. M.; Lucci, F. R.; Lee, S.; Michaelides, A.; Flytzani-Stephanopoulos, M.; Stamatakis, M.; Sykes, E. C. H. Pt/Cu Single-Atom Alloys as Coke-Resistant Catalysts for Efficient C–H Activation. *Nat. Chem.* **2018**, *10*, 325.
- (10) Sun, G.; Zhao, Z.-J.; Mu, R.; Zha, S.; Li, L.; Chen, S.; Zang, K.; Luo, J.; Li, Z.; Purdy, S. C.; Kropf, A. J.; Miller, J. T.; Zeng, L.; Gong, J. Breaking the Scaling Relationship via Thermally Stable Pt/Cu Single Atom Alloys for Catalytic Dehydrogenation. *Nat. Commun.* **2018**, *9*, 4454.
- (11) Wang, Z.-T.; Hoyt, R. A.; El-Soda, M.; Madix, R. J.; Kaxiras, E.; Sykes, E. C. H. Dry Dehydrogenation of Ethanol on Pt-Cu Single Atom Alloys. *Top. Catal.* **2018**, *61*, 328-335.
- (12) Aich, P.; Wei, H.; Basan, B.; Kropf, A. J.; Schweitzer, N. M.; Marshall, C. L.; Miller, J. T.; Meyer, R. Single-Atom Alloy Pd–Ag Catalyst for Selective Hydrogenation of Acrolein. *J. Phys. Chem.* C **2015**, *119*, 18140–18148.
- (13) Lucci, F. R.; Liu, J.; Marcinkowski, M. D.; Yang, M.; Allard, L. F.; Flytzani-Stephanopoulos, M.; Sykes, E. C. H. Selective Hydrogenation of 1,3-Butadiene on Platinum—Copper Alloys at the Single-Atom Limit. *Nat. Commun.* **2015**, *6*, 8550.
- (14) Yang, K.; Yang, B. Identification of the Active and Selective Sites over a Single Pt Atom-Alloyed Cu Catalyst for the Hydrogenation of 1,3-Butadiene: A Combined DFT and Microkinetic Modeling Study. *J. Phys. Chem. C* **2018**, *122*, 10883–10891.
- (15) Lv, C.-Q.; Liu, J.-H.; Guo, Y.; Wang, G.-C. Selective Hydrogenation of 1,3-Butadiene over Single Pt1/Cu(1 1 1) Model Catalysts: A DFT Study. *Appl. Surf. Sci.* **2019**, *466*, 946–955.

- (16) Cao, Y.; Chen, B.; Guerrero-Sánchez, J.; Lee, I.; Zhou, X.; Takeuchi, N.; Zaera, F. Controlling Selectivity in Unsaturated Aldehyde Hydrogenation Using Single-Site Alloy Catalysts. *ACS Catal.* **2019**, *9*, 9150–9157.
- (17) Gallezot, P.; Richard, D. Selective Hydrogenation of α,β-Unsaturated Aldehydes. *Catal. Rev.: Sci. Eng.* **1998**, 40, 81–126.
- (18) Mäki-Arvela, P.; Hájek, J.; Salmi, T.; Murzin, D. Y. Chemoselective Hydrogenation of Carbonyl Compounds over Heterogeneous Catalysts. *Appl. Catal.*, A 2005, 292, 1–49.
- (19) Yuan, Y.; Yao, S.; Wang, M.; Lou, S.; Yan, N. Recent Progress in Chemoselective Hydrogenation of α,β -Unsaturated Aldehyde to Unsaturated Alcohol over Nanomaterials. *Curr. Org. Chem.* **2013**, *17*, 400–413.
- (20) Kyriakou, G.; Boucher, M. B.; Jewell, A. D.; Lewis, E. A.; Lawton, T. J.; Baber, A. E.; Tierney, H. L.; Flytzani-Stephanopoulos, M.; Sykes, E. C. H. Isolated Metal Atom Geometries as a Strategy for Selective Heterogeneous Hydrogenations. *Science* **2012**, 335, 1209–1212.
- (21) Lucci, F. R.; Marcinkowski, M. D.; Lawton, T. J.; Sykes, E. C. H. H₂ Activation and Spillover on Catalytically Relevant Pt–Cu Single Atom Alloys. *J. Phys. Chem. C* **2015**, *119*, 24351–24357.
- (22) Lucci, F. R.; Darby, M. T.; Mattera, M. F. G.; Ivimey, C. J.; Therrien, A. J.; Michaelides, A.; Stamatakis, M.; Sykes, E. C. H. Controlling Hydrogen Activation, Spillover, and Desorption with Pd–Au Single-Atom Alloys. *J. Phys. Chem. Lett.* **2016**, *7*, 480–485.
- (23) Therrien, A. J.; Hensley, A. J. R.; Marcinkowski, M. D.; Zhang, R.; Lucci, F. R.; Coughlin, B.; Schilling, A. C.; McEwen, J.-S.; Sykes, E. C. H. An Atomic-Scale View of Single-Site Pt Catalysis for Low-Temperature CO Oxidation. *Nat. Catal.* **2018**, *1*, 192–198.
- (24) Darby, M. T.; Réocreux, R.; Sykes, E. C. H.; Michaelides, A.; Stamatakis, M. Elucidating the Stability and Reactivity of Surface Intermediates on Single-Atom Alloy Catalysts. *ACS Catal.* **2018**, *8*, 5038–5050.
- (25) Darby, M. T.; Stamatakis, M.; Michaelides, A.; Sykes, E. C. H. Lonely Atoms with Special Gifts: Breaking Linear Scaling Relationships in Heterogeneous Catalysis with Single-Atom Alloys. *J. Phys. Chem. Lett.* **2018**, *9*, 5636–5646.
- (26) Somorjai, G. A.; Li, Y. Introduction to Surface Chemistry and Catalysis, 2nd ed.; John Wiley & Sons: New York, 2010.
- (27) Oxford, S. M.; Lee, P. L.; Chupas, P. J.; Chapman, K. W.; Kung, M. C.; Kung, H. H. Study of Supported PtCu and PdAu Bimetallic Nanoparticles Using In-Situ X-Ray Tools. *J. Phys. Chem. C* **2010**, *114*, 17085—17091.
- (28) Andersson, K. J.; Calle-Vallejo, F.; Rossmeisl, J.; Chorkendorff, I. Adsorption-Driven Surface Segregation of the Less Reactive Alloy Component. J. Am. Chem. Soc. 2009, 131, 2404–2407.
- (29) Simonovis, J. P.; Hunt, A.; Palomino, R. M.; Senanayake, S. D.; Waluyo, I. Enhanced Stability of Pt-Cu Single-Atom Alloy Catalysts: In Situ Characterization of the Pt/Cu(111) Surface in an Ambient Pressure of CO. *J. Phys. Chem. C* **2018**, *122*, 4488–4495.
- (30) Gumuslu, G.; Kondratyuk, P.; Boes, J. R.; Morreale, B.; Miller, J. B.; Kitchin, J. R.; Gellman, A. J. Correlation of Electronic Structure with Catalytic Activity: H_2 – D_2 Exchange across Cu_xPd_{1-x} Composition Space. *ACS Catal.* **2015**, *5*, 3137–3147.
- (31) Weng, Z.; Zaera, F. Sub-Monolayer Control of Mixed-Oxide Support Composition in Catalysts via Atomic Layer Deposition: Selective Hydrogenation of Cinnamaldehyde Promoted by (SiO₂-ALD)-Pt/Al₂O₃. ACS Catal. **2018**, *8*, 8513–8524.
- (32) Yao, Y.; Guerrero-Sánchez, J.; Takeuchi, N.; Zaera, F. Coadsorption of Formic Acid and Hydrazine on Cu(110) Single-Crystal Surfaces. *J. Phys. Chem. C* **2019**, *123*, 7584–7593.
- (33) Guerrero-Sánchez, J.; Takeuchi, N.; Zaera, F. Density Functional Theory Study of the Surface Adsorption and Dissociation of Copper(I) Acetamidinates on Cu(110) Surfaces. *J. Phys. Chem. C* **2019**, *123*, 4341–4348.
- (34) Kresse, G.; Furthmüller, J. Efficient Iterative Schemes for Ab Initio Total-Energy Calculations Using a Plane-Wave Basis Set. *Phys. Rev. B: Condens. Matter Mater. Phys.* **1996**, 54, 11169–11186.

- (35) Blöchl, P. E. Projector Augmented-Wave Method. Phys. Rev. B: Condens. Matter Mater. Phys. 1994, 50, 17953-17979.
- (36) Perdew, J. P.; Burke, K.; Ernzerhof, M. Generalized Gradient Approximation Made Simple. *Phys. Rev. Lett.* **1996**, *77*, 3865–3868.
- (37) Grimme, S.; Antony, J.; Ehrlich, S.; Krieg, H. A Consistent and Accurate Ab Initio Parametrization of Density Functional Dispersion Correction (DFT-D) for the 94 Elements H-Pu. *J. Chem. Phys.* **2010**, 132, 154104.
- (38) Bond, G. C. Metal-Catalysed Reactions of Hydrocarbons; Springer: New York, 2005.
- (39) Zaera, F. Key Unanswered Questions About the Mechanism of Olefin Hydrogenation Catalysis by Transition-Metal Surfaces: A Surface-Science Perspective. *Phys. Chem. Chem. Phys.* **2013**, *15*, 11988–12003.
- (40) Dong, Y.; Zaera, F. Selectivity in Hydrogenation Catalysis with Unsaturated Aldehydes: Parallel Versus Sequential Steps. *J. Phys. Chem. Lett.* **2018**, *9*, 1301–1306.
- (41) Davis, S. M.; Zaera, F.; Somorjai, G. A. The Reactivity and Composition of Strongly Adsorbed Carbonaceous Deposits on Platinum. Model of the Working Hydrocarbon Conversion Catalyst. *J. Catal.* **1982**, *77*, 439.
- (42) Ma, Z.; Zaera, F. Organic Chemistry on Solid Surfaces. *Surf. Sci. Rep.* **2006**, *61*, 229–281.
- (43) Zaera, F. The Surface Chemistry of Metal-Based Hydrogenation Catalysis. ACS Catal. 2017, 7, 4947–4967.
- (44) Simonovis, J.; Tillekaratne, A.; Zaera, F. The Role of Carbonaceous Deposits in Hydrogenation Catalysis Revisited. *J. Phys. Chem. C* **2017**, 121, 2285–2293.
- (45) Zaera, F. Study of the Surface Chemistry of Ethyl Groups on Pt(111) by Using Partially Deuterated Ethyl Iodide. *J. Phys. Chem.* **1990**, *94*, 8350–8355.
- (46) Zaera, F. Preparation and Reactivity of Alkyl Groups Adsorbed on Metal Surfaces. Acc. Chem. Res. 1992, 25, 260–265.
- (47) Zaera, F. On the Mechanism for the Hydrogenation of Olefins on Transition-Metal Surfaces: The Chemistry of Ethylene on Pt(111). *Langmuir* 1996, 12, 88–94.
- (48) Singh, U. K.; Vannice, M. A. Kinetics of Liquid-Phase Hydrogenation Reactions over Supported Metal Catalysts a Review. *Appl. Catal., A* **2001**, 213, 1–24.
- (49) Loffreda, D.; Delbecq, F.; Vigne, F.; Sautet, P. Chemo-Regioselectivity in Heterogeneous Catalysis: Competitive Routes for C = O and C = C Hydrogenations from a Theoretical Approach. *J. Am. Chem. Soc.* **2006**, *128*, 1316–1323.
- (50) Yang, B.; Wang, D.; Gong, X.-Q.; Hu, P. Acrolein Hydrogenation on Pt(211) and Au(211) Surfaces: A Density Functional Theory Study. *Phys. Chem. Chem. Phys.* **2011**, *13*, 21146–21152.
- (51) Sitthisa, S.; Sooknoi, T.; Ma, Y.; Balbuena, P. B.; Resasco, D. E. Kinetics and Mechanism of Hydrogenation of Furfural on Cu/SiO₂ Catalysts. *J. Catal.* **2011**, *277*, 1–13.
- (52) Cao, X.-M.; Burch, R.; Hardacre, C.; Hu, P. Reaction Mechanisms of Crotonaldehyde Hydrogenation on Pt(111): Density Functional Theory and Microkinetic Modeling. *J. Phys. Chem. C* **2011**, *115*, 19819–19827.
- (53) Ide, M. S.; Hao, B.; Neurock, M.; Davis, R. J. Mechanistic Insights on the Hydrogenation of α,β -Unsaturated Ketones and Aldehydes to Unsaturated Alcohols over Metal Catalysts. *ACS Catal.* **2012**, *2*, 671–683.
- (54) Stolle, A.; Gallert, T.; Schmoger, C.; Ondruschka, B. Hydrogenation of Citral: A Wide-Spread Model Reaction for Selective Reduction of α , β -Unsaturated Aldehydes. *RSC Adv.* **2013**, 3, 2112–2153
- (55) Kennedy, G.; Baker, L. R.; Somorjai, G. A. Selective Amplification of C(O Bond Hydrogenation on Pt/TiO₂: Catalytic Reaction and Sum-Frequency Generation Vibrational Spectroscopy Studies of Crotonaldehyde Hydrogenation. *Angew. Chem., Int. Ed.* **2014**, *53*, 3405–3408.
- (56) Dong, Y.; Ebrahimi, M.; Tillekaratne, A.; Simonovis, J. P.; Zaera, F. Hydrogenation vs. H-D Isotope Scrambling During the Conversion of Ethylene with Hydrogen/Deuterium Catalyzed by

- Platinum under Single-Collision Conditions. Phys. Chem. Chem. Phys. 2016, 18, 19248–19258.
- (57) Dong, Y.; Zaera, F. Kinetics of Hydrogen Adsorption During Catalytic Reactions on Transition Metal Surfaces. *Catal. Sci. Technol.* **2017**, *7*, 5354–5364.
- (58) Giannakakis, G.; Flytzani-Stephanopoulos, M.; Sykes, E. C. H. Single-Atom Alloys as a Reductionist Approach to the Rational Design of Heterogeneous Catalysts. *Acc. Chem. Res.* **2019**, *52*, 237–247.
- (59) Luneau, M.; Shirman, T.; Foucher, A. C.; Duanmu, K.; Verbart, D. M. A.; Sautet, P.; Stach, E. A.; Aizenberg, J.; Madix, R. J.; Friend, C. M. Achieving High Selectivity for Alkyne Hydrogenation at High Conversions with Compositionally Optimized PdAu Nanoparticle Catalysts in Raspberry Colloid-Templated SiO₂. ACS Catal. **2020**, 10, 441–450.
- (60) Kittel, C. Introduction to Solid State Physics, 8th ed.; John Wiley & Sons: New York, 2005.
- (61) Nørskov, J. K.; Studt, F.; Abild-Pedersen, F.; Bligaard, T. Fundamental Concepts in Heterogeneous Catalysis. In *Fundamental Concepts in Heterogeneous Catalysis*; Wiley Blackwell, 2014; Vol. 9781118888957; pp 114–137.
- (62) Xin, H.; Vojvodic, A.; Voss, J.; Nørskov, J. K.; Abild-Pedersen, F. Effects of D-Band Shape on the Surface Reactivity of Transition-Metal Alloys. *Phys. Rev. B: Condens. Matter Mater. Phys.* **2014**, 89, 115114.
- (63) Andersen, M.; Medford, A. J.; Nørskov, J. K.; Reuter, K. Scaling-Relation-Based Analysis of Bifunctional Catalysis: The Case for Homogeneous Bimetallic Alloys. *ACS Catal.* **2017**, *7*, 3960–3967.